

HOSTED BY



ELSEVIER

Contents lists available at ScienceDirect

Progress in Natural Science: Materials International

journal homepage: www.elsevier.com/locate/pnsmi

Review

Gas-Solution Interface Technique as a simple method to produce inorganic microtubes with scroll morphology

Larisa B. Gulina^{a,*}, Valeri P. Tolstoy^a, Alexander A. Solov'ev^b, Vladislav E. Gurenko^a, Gaoshan Huang^b, Yongfeng Mei^b^a Department of Solid State Chemistry, Saint-Petersburg State University, 7/9 Universitetskaya nab., St. Petersburg, 199034, Russia^b Department of Materials Science, Fudan University, 220 Handan Road, Shanghai, 200433, China

ARTICLE INFO

Keywords:

Interface
Rolled-up microtubes
2D nanocrystals
Inorganic machines
Nanomaterials

ABSTRACT

Over the past decade, numerous studies have dealt with new properties of inorganic nanomaterials with improved characteristics due to a particular morphology, and new facile methods to produce such materials have been reported. Inorganic microtubes can be designed for multifunctional materials with highly specific surface area. These microtubes can act as individual on-chip components of miniature devices or off-chip micro-machines. The paper first discusses the main regularities of the reactions at the gas-solution interface and then goes on to present the basic principles of the Gas-Solution Interface Technique (GSIT), thus demonstrating a new way of facile synthesis of inorganic rolled-up microtubes. A distinctive feature of the technique is the formation of a gradient solid layer on the surface of the aqueous solution as a result of the gaseous and liquid reagents interaction. When dried in the air, this thin layer is capable of self-folding into microtubes with specific morphology. The paper considers the specific features of microtubes obtained by GSIT from numerous classes of inorganic compounds, including oxides, hydroxides, sulfides, fluorides. Further areas of possible practical applications of GSIT microtubes are discussed. The prospects of future development of the GSIT are outlined.

1. Introduction

Tubes are widely used in advanced systems, which integrate the geometry and functions of materials to produce new devices, such as powerful jet engines and pipes to transport fuels, exchange heat and generate steam [1]. In biology, hundreds of miles of tubes – veins, arteries, capillaries – supply nutrients, exchange metabolic products and support all the essential functions of the human body. In the last decade, there has been great interest in the study of tubes with micro- and nanoscale diameters. At the sub-micro scale, one can study and utilize a large number of materials properties [2,3]. However, conventional micromechanical fabrication methods cannot be used to produce tubes with ultra-thin walls and diameters below 1 mm. At the same time, microelectronic technology, which deals with the growth and fabrication of planar structures, can only be applied to the construction of more complex three-dimensional planar micro-devices. Therefore, the development of new paradigm-shift methods of fabricating three-dimensional tubular microstructures with tunable diameters, controllable thicknesses of walls and given geometric parameter ratios is very important for advanced materials. Nowadays, approaches of microtubes fabrication are expanding to new methods and materials,

such as rolling up of polymer films [4], self-assembly of biological material [5], lithography [6] and additive manufacturing [7]. Other techniques include template-assisted approach [8–10], vapor deposition [11], hydrothermal synthesis [12,13], sol-gel non-template synthesis [14], controlled etching [15] and Kirkendall effect [16]. However, only a few methods can be used to scale-up the fabrication of microtubes due to long-term experimental procedures. Moreover, obtaining tubes with ultrathin walls is crucial to explore the novel fundamental quantum, chemical, electronic and optical properties of 3D nanomaterials [17].

The era of strain-engineered rolled-up 3D nanotechnology started approximately two decades ago from an observation of self-rolling up process of strain-engineered heteroepitaxial nanolayers into nano-/microtubes [18]. This methodology helped to obtain a novel class of quantum and multifunctional semiconductor microtubes [19]. Particular attention was paid to silicon and germanium nano-membranes due to their high potential in designing the next generation of micro-electronic devices [20,21]. A decade later, the rolled-up nanotech on polymers (e.g., photoresist) helped to obtain a new generation of microtubes based on the polycrystalline nano-membranes comprising metals, oxides and/or semiconductors [22].

* Corresponding author.

E-mail address: l.gulina@spbu.ru (L.B. Gulina).<https://doi.org/10.1016/j.pnsc.2020.05.001>

Received 27 August 2019; Received in revised form 1 May 2020; Accepted 9 May 2020

Available online 22 July 2020

1002-0071/ © 2020 Chinese Materials Research Society. Published by Elsevier B.V. This is an open access article under the CC BY-NC-ND license (<http://creativecommons.org/licenses/by-nc-nd/4.0/>).

3D nanomaterials showed great promise in terms of multiple potential on-chip (tube free standing/integrated on surface) and off-chip (tubes released in solution) applications. For instance, mechanical conjugated polypyrrole-gold actuators can self-roll and unroll simply by varying the values of voltage [23] and thus serve as prototype elements for integration in nano-/micro-electro-mechanical systems (NEMS or MEMS). Rolled-up microtubes can also play the role of stimuli-responsive sensors for the detection of specific gases and liquids [24]. Enhanced photocatalytic generation of hydrogen gas was demonstrated using graphitic carbonitride ($g\text{-C}_3\text{N}_4$) tubes, which contain multiple active sites for proton reduction and electron transfer [25]. Azimutal magnetized microtubes consisting of metallic nanomembranes can have useful applications in magneto-impedance-based field sensors [26]. Moreover, on-chip integrated microtubes play the role of new electronic components, such as supercapacitors for energy storage [27], fluidic transistors [28] and inductors [29]. In addition, when located in chemical fuels microtubes containing internal catalytic layers (e.g., Pt, Ag) can operate as highly efficient tubular nano-/micromotors [30]. Recently, particular attention has been given to the study of electromagnetic waves (whispering-gallery mode) propagating in optical microcavity with tubular geometry, i.e. optical micro-resonators, which can be used as sensitive chemical sensors [31,32].

In a series of works by L. Gulina and V. Tolstoy [33–38] it was demonstrated that the conditions required to form “rolled-up” inorganic structures could be created if planar thin layers were obtained using Gas-Solution Interface Technique (GSIT), i.e. as a result of chemical reactions between two reagents, one of which is gaseous, and the other is dissolved in a liquid. During the reactions, a thin gradient film is formed due to the spatial separation of the reagents and their diffusion at the interface. In this way, gradients in thin films can arise from the difference in morphology, density, and/or chemical composition of the film surfaces. Subsequently, under certain conditions the presence of these gradients causes the emergence of interfacial forces, which “roll-up” the initial planar layers, in particular during the drying of thin films.

However, it is obvious that the magnitudes of the forces necessary for the formation of the microtubes depend strongly on many factors, including the thicknesses and densities of the thin films, their elastic moduli, wetting angles, adsorption capacity with respect to the reagents, the gradients and related parameters. Moreover, many of these parameters are determined by the conditions of synthesis, which include the concentrations of reagents and time of their interaction, the presence of background electrolyte in solutions, etc. For a more complete description of such processes at the interface, it is necessary to take into account the laws of gas absorption in solvents and the formation and growth of nanoscale crystals that can form such thin films at the gas-liquid interface. It is important to determine synthetic conditions, which assist facile producing of inorganic microtubes with scroll morphology. In the current work, the possibilities of GSIT to obtain tubular structures are observed for the first time.

Based on the most studied reactions, the aim of our review is a detailed and complete summary, bringing together the results obtained in the area of microtubes synthesis by GSIT, followed by experimental examples, theoretical considerations and discussion of the further prospects of the method developed.

2. Formation of thin film and crystals at gas-liquid interface

2.1. Basic laws of gas diffusion through gas-liquid interface

For a complete description of gases adsorption, dissolution of and subsequent chemical reaction processes, it is usually necessary to solve together the equations of diffusion, convective transport and chemical kinetics, which can be very difficult. Therefore, in practice, simplified models are used, which can be well confirmed by experimental data.

The two-film model [39] postulates that the gas transfers through the interface via stationary molecular diffusion in a hypothetical two-film stagnant system: gas and solution films with thicknesses of δ_{gas} and

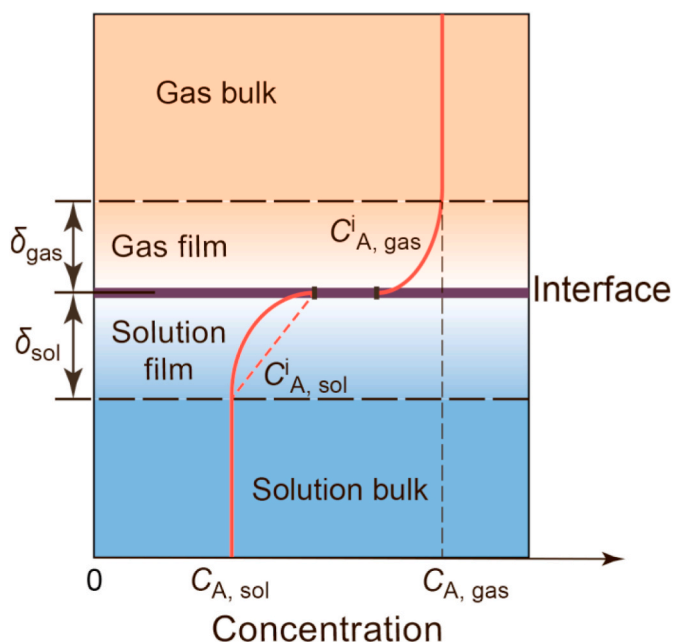


Fig. 1. Schematic representation of gas-solution system showing the two-film model and its concentration profile for the component A (dashed line stands for the linear concentration drop in the liquid film, when no reaction between the gas and solution occurs).

δ_{sol} , respectively. All resistance to mass transport is located in this system (which is in equilibrium), so the concentration gradients change only there. The concentrations in the bulk gas and solution are constant since they are well mixed (Fig. 1).

The specific rate of absorption (R) can be described as the amount of component A transferred from the gas to the interface or, in other words, the amount relocated from the interface to the solution:

$$R = k_{\text{gas}}(C_{\text{A gas}} - C_{\text{A gas}}^i) = k_{\text{sol}}(C_{\text{A sol}}^i - C_{\text{A sol}}) \quad (1.1)$$

where k_{gas} , k_{sol} – gas and solution mass transfer coefficients, $C_{\text{A sol}}$, $C_{\text{A sol}}^i$ – bulk and interfacial solution concentrations of the component A. The irreversible chemical reaction (with k_2 reaction rate) between the gas A and the solution component B can be modeled using the following stoichiometry:



The influence of this reaction should be implemented into Equation (1.1) by the enhancement factor E_a . It shows how much the physical absorption is augmented by the chemical reaction at the same concentration gradient. For reaction 1.2, the E_a is a function of two parameters: the enhancement factor of the instant reaction (E_{inf}) and the Hatta number (Ha), which reproduces the ratio between the amount of the component A consumed in the solution by the film and the amount of A transferred in the absence of a chemical reaction [40].

Three boundary cases of absorption exist, depending on the Ha value and Ha/E_{inf} ratio:

1) Fast pseudo-first order regime (Fig. 2a)

In this case, the B component is in excess in comparison with the gaseous A, so its concentration is constant in the bulk and solution film. The following interval satisfies this regime:

$$2 \ll Ha \ll E_{\text{inf}} \quad (1.3)$$

The solution film interfacial flux of the component A (gas absorption) can be written as:

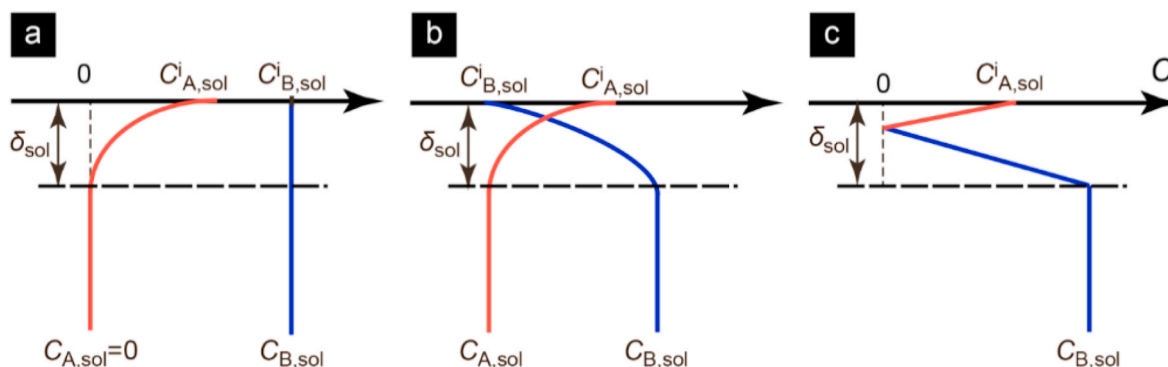


Fig. 2. Three cases of absorption with chemical reaction: (a) – a fast pseudo-first order regime; (b) – an intermediate regime; (c) – instantaneous reaction in the solution film.

$$N_{A\ sol} = \sqrt{k_{ov} D_A C_{A\ sol}^i} \quad (1.4)$$

where k_{ov} is the overall reaction rate constant defined as $k_{ov} = k_2 C_{B\ sol}$. The experimental data of the absorption rate can directly point at the kinetic rate constant if Henry's constant and diffusivity are known.

2) Intermediate regime (Fig. 2b)

When the gas concentration at the interface increases, a depletion of the component B begins. This decreases the E_{inf} and makes it possible to obtain the kinetic rate only by numeric approximations.

3) Instantaneous reaction (Fig. 2c)

This regime does not allow the determination of the mass transfer rate or the kinetics from the experimental data: the rate of the chemical reaction is infinitely high in comparison with the absorption.

Despite the fact that the film model is mathematically simple, the δ_{gas} and δ_{sol} parameters are hard to be predicted as they depend on the physical properties and geometry of the system under consideration.

2.2. Interaction at the gas-liquid interface

To form a solid thin film, the system has to pass through a nucleation stage. As shown by Gibbs, the nucleus is formed from an ambient phase, and it is crucial to have a cluster of “building blocks” that comes from the supersaturated solution. Supersaturation is achieved by various methods, which include evaporation of the solvent, cooling/heating the solution, pH shift, etc.

Ignoring the anisotropy and assuming that the solid spherical nuclei contain a number of atoms and possess a radius r , the change of Gibbs free energy by nucleus formation can be written as:

$$\Delta G = -\left(\frac{4\pi r^3}{3\Omega}\right)\Delta\mu + 4\pi r^2\gamma \quad (2.1)$$

where $\Delta\mu$ – change of chemical potential for the particle to transfer from the liquid to solid phase, γ – nucleus interfacial free energy. The number of atoms is approximated from the ratio between the full nucleus volume ($4\pi r^3/3$) and one-particle volume (Ω), the nucleus area equals $4\pi r^2$.

The critical size r^* can be calculated from the extreme point, where $d\Delta G/dr$ reaches zero:

$$r^* = \frac{2\Omega\gamma}{\Delta\mu} \quad (2.2)$$

Normally, two situations are possible. If the cluster size is lower than the critical value ($r < r^*$), then the nucleus dissolves spontaneously. Conversely, if the size is greater than the critical value, the cluster grows increasing its overall energy. Eventually, the nuclei

transform into a crystal through different growth mechanisms.

It is assumed that when the crystallization at the gas-solution interface occurs, several nuclei might appear on the surface of the solution supported by its surface tension. They will spread along the surface and finally run into each other and merge.

Several examples of solid compounds formed as a result of interfacial deposition on a solution surface are listed in Table 1.

The literature review allows us to highlight three possible modes of solids formation at the gas-solution interface.

- 1) The concentrations of the interacting components A and B are sufficient to form nuclei. The stage limiting the reaction rate is the diffusion of the components into the reaction zone. In this case, the reaction products include nanoparticles or nanocrystals, often with unconventional morphology. The most probable mechanism for product formation at the interface is a nucleation-growth-assembly process.
- 2) Intermediate mode. The diffusion rate and the rate of solid deposition at the interface differ slightly, so the formation of a non-continuous porous film or network on the surface is possible. The reaction in the open areas of the solution surface continues inward if there is no restriction in the diffusion of the reagents. In this mode, it is possible to determine a narrow range of experimental synthetic conditions that lead to the formation of a thick solid gradient film that can curl and transform into scrolls. Gradient can be manifested as a difference in chemical composition or physical characteristics (density, internal strain, humidity) between two surfaces of the film. When dried, such a double film will relax inward or outward, resulting in the transformation into scroll.
- 3) The concentrations of the components A and B in the reaction zone are sufficient for the rapid formation of a planar continuous thin film at the interface. The interaction between the components stops because a continuous film prevents their diffusion. Another variant of this technique is the formation of a thin Langmuir film with its further chemical transformation. Such reactions are not considered in this review.

It should be noted that in all the above-mentioned cases it is possible to use surfactants, organic or bio-molecules as templates.

3. Formation of inorganic microtubes at the gas-liquid interface

3.1. Surfactant-assisted synthesis

Within the scope of this review we consider some experimental studies that report microtubular structures formation. As can be noted, there are a few works describing the formation of microtubes at the interface. In most of the cases, surfactants and templates must be used in these processes. For example, (i) it was demonstrated [57] that the

Table 1
Inorganic thin films and crystals synthesized at the liquid-gas interface.

Product	Gaseous reagent	Solution	The reaction peculiarities	Ref.
SiO ₂ (Fig. 3a)		Tetraethoxysilane, cetylpyridinium chloride	Hydrolysis and condensation.	[41]
Zn(INA) ₂ (H ₂ O) ₄ (INA - isonicotinate)	NH ₃	Zn(NO ₃) ₂ , isonicotinic acid	Kinetically controlled NH ₃ vapor diffusion.	[42]
ZnO	NH ₃	Zn(NO ₃) ₂	Hydrolysis and condensation.	[43]
CuO	NH ₃	Cu(NO ₃) ₂	The sequence of transformations is Cu ²⁺ → Cu ₂ (OH) ₂ NO ₃ → Cu(OH) ₂ → Cu(OH) ₄ ²⁻ → CuO.	[44]
Fe ₃ O ₄	NH ₃	FeCl ₃ and FeSO ₄ mixed solution with a molar ratio of 3:2	Separation in magnetic field was employed to extract the product.	[45]
Mg(OH) ₂	NH ₃	MgCl ₂	The formation mechanism of the vertically aligned nanosheets at the interface is a nucleation-growth-assembly process.	[46]
Ni(OH) ₂	NH ₃	NiSO ₄	The nucleation, coalescence, oriented attachment, Ostwald ripening, and further crystal growth occurred at the interface.	[47]
MnO ₂	CH ₂ O	MnCl ₂ , EDTA, NaOH, K ₂ S ₂ O ₈	The MnO ₂ dispersion have been modified by CH ₂ O.	[48]
Pt	CH ₂ O	H ₂ PtCl ₆ ·6H ₂ O, chitosan	Reaction was performed under stirring. A gas-liquid interface forms when volatilized methyl aldehyde gas dissolves in solution, and metal ions begin to be reduced slowly at the surface of the solution.	[49]
Ag	CH ₃ CHO	AgNO ₃ , NH ₄ OH, Na ₃ C ₆ H ₅ O ₇ , NaBH ₄	First, the solution containing silver seeds was prepared, and then a reaction with volatilized CH ₃ CHO was performed for 3 h at room temperature with continuous magnetic stirring.	[50]
Ag	N ₂ H ₄	AgOAc, NH ₄ OAc	The nucleation, anisotropic crystal growth and oriented attachment leads to formation of giant 2D crystals at the interface.	[51]
Ag	N ₂ H ₄	AgNO ₃ , citric acid, NH ₄ OH	The nucleation, crystal growth and aggregation leads to formation of nanoflowers on the solution surface.	[52]
SB ₂ S ₃	H ₂ S	SbCl ₃	The formation of the uniform large-area film at the interface is a nucleation – crystal growth – assembly process.	[53]
Bi ₂ S ₃	H ₂ S	Bi(NO ₃) ₃ , HNO ₃	The sequence of transformations is Bi(NO ₃) ₃ → BIONO ₃ → BIOSH → Bi ₂ S ₃ .	[54]
Bi ₂ O ₃ /Bi ₂ S ₃	NH ₃ , (NH ₄) ₂ S	Bi(NO ₃) ₃ , HNO ₃ , sodium dodecyl sulfate	Hydrolysis and partial sulfuration.	[55]
PbS	H ₂ S	PbCl ₂ , arachidic acid	Triangular single-crystalline nanorings	[56]

polymerization and growth of silicate micellar assemblies at the air–water interface in the presence of surfactants can lead to tubular structures formation (Fig. 3e and f); (ii) curly nickel carbonate hydrate tubular structures can be prepared [58] through a facile drying process of the films formed at the air-solution interface in the presence of a double hydrophilic copolymer or polyelectrolyte additives (Fig. 3g and h); (iii) Co(CO₃)_x(OH)_y tubular structures can be obtained by interfacial mineralization [59] in the presence of a tobacco mosaic virus (TMV) as a versatile template (Fig. 3i and j), and then they can be readily converted to a spinel-type Co₃O₄ tube by annealing at 400 °C.

3.2. Inorganic microtube synthesis without surfactants

Essentially the GSIT method is based on the formation of a layer of insoluble compound as a result of interfacial interaction at the liquid-gas interface. A distinctive feature of the method is the use of pure aqueous solutions without the use of templates. This allows obtaining nano- and microstructured tubular material that is not contaminated with organic impurities. The scheme of the GSIT operations is shown in Fig. 4.

3.2.1. Synthesis of sulfide microtubes by thiosalt decomposition

The first experiments of sulfide microtube synthesis by the GSIT method were performed using As₂S₃ [33] and AgAsS₂ [60]. The aqueous solution of NaAsS₂ and gaseous HCl were used as reagents. The experiments showed that a yellow-colored layer was formed on the solution surface as a result of thiosalt decomposition due to solution acidification. After washing the layer was placed on a silicon substrate and dried in the air. During drying a number of microtubes ranging from 20 to 100 μm in diameter and up to 2 mm long were formed (Fig. 5a and b). Raman spectroscopy (Fig. 5c) showed an absorption band at 342 cm⁻¹, which can be attributed to the oscillations of the As–S bonds [61], with the intensity being greater on the inside than on the outside. In our opinion, the result suggests that the synthesized layer has a difference in the state of the two surfaces, for example, in terms of roughness/smoothness. A very important task was to determine the direction of rolling of the synthesized interfacial layer. In order to do this, the synthesized As₂S₃ layer, after the washing stage, was transferred to the surface of the AgNO₃ solution for 20 min. After a subsequent double washing from excess silver salt solution, the layer was transferred to the silicon surface and dried at room temperature. As a result, microtubes are formed with diameters of up to 100 μm and lengths up to 3 mm (Fig. 5d). The tube wall with a thickness of about 2 μm has a well-defined gradient of density: surfaces that are smooth inside and spongy outside (Fig. 5e). The results of the investigation by Electron Probe Micro Analysis (EPMA) are shown in Fig. 5f. The data indicate that silver is localized mainly on the outside surface of the tube wall. This fact shows that the direction of twisting corresponds to the scheme presented in Fig. 5g, namely, the surface of the layer from the gaseous phase is transformed into the inner surface of the microtube.

3.2.2. Synthesis of oxide microtubes as a result of reaction with ozone

In Ref. [62], it was first shown that it was possible to obtain similar microtubular structures of oxides, for example, through the interaction of gaseous ozone with the surface of an aqueous solution of manganese salt. A detailed study of the influence of the composition of the solution on the crystal structure of the products of interaction was made in Refs. [38]. It was demonstrated that as a result of a reaction for 2–10 min, a film with crystalline structure of birnessite is formed at the interface and transformed into microtubes by drying (Fig. 6a and b). For a sample with a wall thickness of less than 1 μm or greater than 4 μm, the formation of microtubes was not observed. In other words, when the thickness is less than 1 μm, microtubes are not formed due to the comparatively low mechanical strength of the synthesized layers; with thicker layers, it is the excessive stiffness that hampers their “rolling up”. A SEM image of the microtubes is presented in Fig. 6b. The image

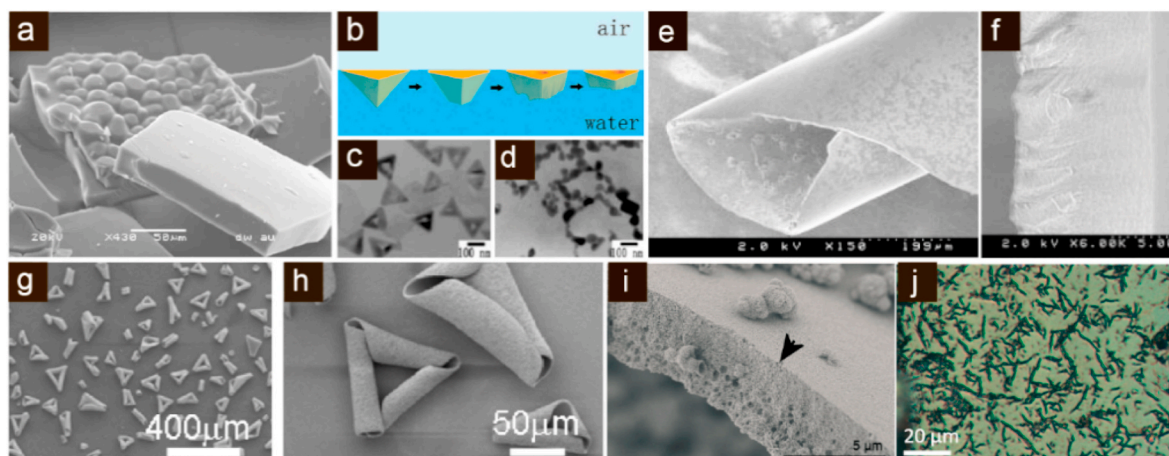


Fig. 3. Examples of inorganic thin film structures synthesized at the air-solution interface: **(a)** SEM image showing top (smooth) and bottom (rough) surfaces of a thick silica-surfactant film grown at the air-solution interface from a dilute acidic solution containing tetramethoxysilane and cetylpyridinium chloride. (a) Reproduced with permission [41]. Copyright 2006, Royal Society of Chemistry. **(b)** Schematic illustration of the formation process of PbS nanorings and **(c, d)** TEM micrographs of PbS nanorings after 2 h (c), and 8 h (d) ripening at the air-water interface. (b–d) Reprinted with permission [56]. Copyright 2009, American Chemical Society. **(e, f)** SEM images of an as-synthesized mesoporous silica film formed at the air-water interface showing (e) a typical surface with bending and (f) cross section with a thickness of ca. 5–10 μm . (e, f) Reproduced with permission [57]. Copyright 1998, Royal Society of Chemistry. **(g, h)** SEM images of curly film consisting of nickel carbonate hydrate synthesized in the presence of the PEG-PEI-(CH_2 -(CH-OH) $_3$ - $\text{CH}_2\text{CONHNH}_2$) $_3$ polymer with different magnification. (g, h) Reprinted with permission [58]. Copyright 2010, American Chemical Society. **(i)** SEM image of an interface-grown $\text{Co}(\text{CO}_3)_x(\text{OH})_y$ film with porous structure after calcination. **(j)** Light microscopy of Co^{2+} /TMV association complexes isolated from a CoCl_2 /TMV solution. (i, j) Reproduced with permission [59]. Copyright 2017, Royal Society of Chemistry.

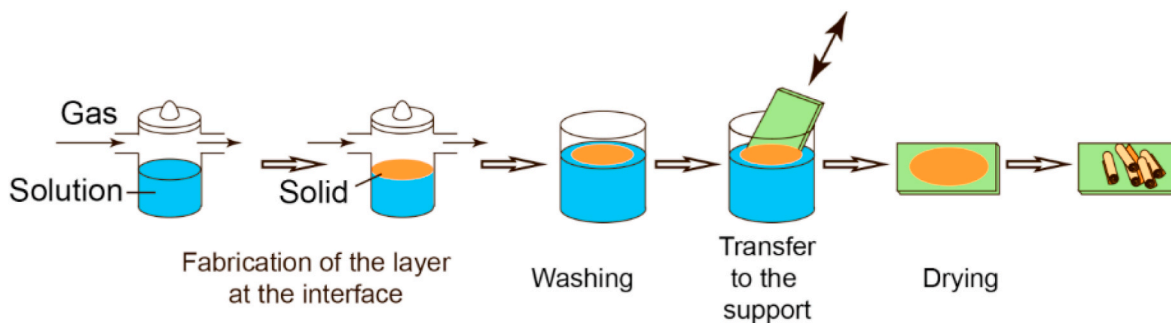


Fig. 4. GSIT scheme for the formation of a solid layer at the solution-air interface and its evolution toward microtubular structures.

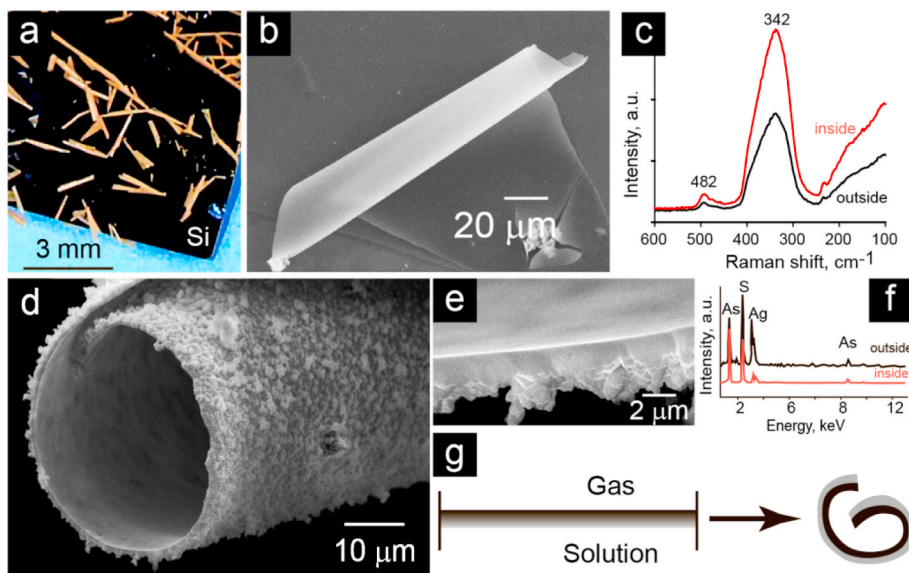


Fig. 5. Examples of sulfide microtubes synthesized at the air-solution interface: **(a)** Optical photo image of As_2S_3 microtubes with 50-fold magnification; **(b)** SEM image of a single As_2S_3 microtube; **(c)** Raman spectra of As_2S_3 microtube wall surfaces: inside (red curve) and outside (black curve); **(d)** SEM image of AgAsS_2 microtube; **(e)** SEM image of cross view of the microtube wall; **(f)** EPMA spectra of the AgAsS_2 microtube wall; **(g)** Hypothetical scheme of the formation of microtubules in the course of drying.

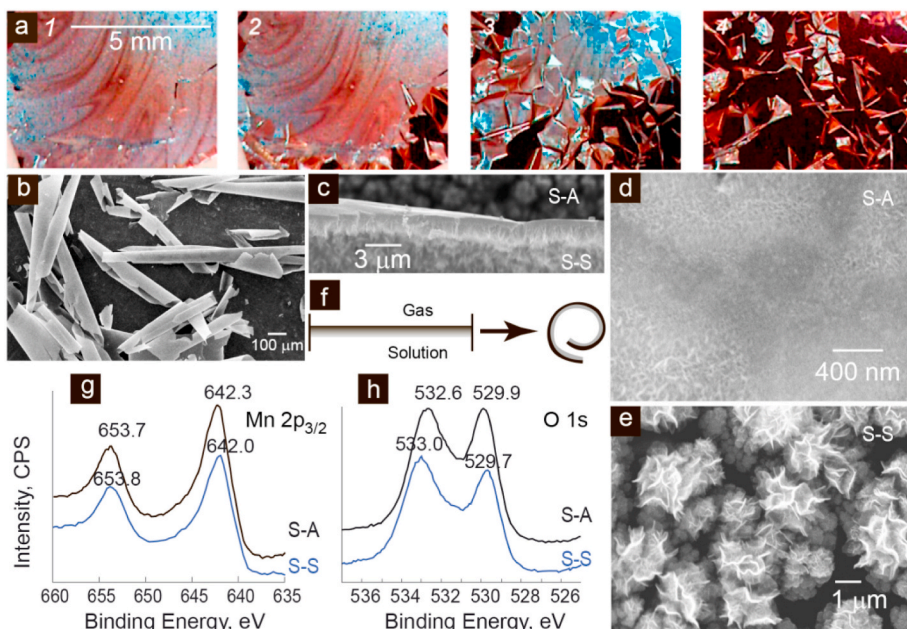


Fig. 6. Experimental results of the synthesis of MnO_2 microtubes. (a) Series of successive images during the spontaneous rolling process. Images 1–4 were taken at 0, 1, 2, and 3 s, respectively. (b–e) SEM images of microtubes: (b) general view, (c) cross view of microtube wall, (d) view of the outer side of microtube, (e) view of the inner side of microtube. (f) Hypothetical scheme of microtube formation in the course of drying. (g, h) XPS spectra of the MnO_2 microtube wall: (g) manganese area; (h) oxygen area. S-A, solid-air interface side; S-S, solid-solution interface side. (a–e, g–h) Reprinted with permission [38]. Copyright 2014, American Chemical Society.

in Fig. 6c indicates that the microtube wall consists of individual nanosheets with a thickness from 2 to 10 nm. From SEM data it is clear that the state of the two surfaces of the tube is different: the side S-A, which was in contact with air during preparation (Fig. 6d), is denser and smoother than the side S-S staying in contact with salt solution (Fig. 6e). It was found (Fig. 6f) that the rolling of the synthesized layer occurs in the following way: the S-A side transforms into the outer tube surface. Fig. 6g and h show the XPS spectra of the microtube wall pertaining to the outer (S-A) and inner (S-S) sides of the microtube. The differences in the spectra are thoroughly discussed in Ref. [38] and the XPS data definitely confirm the higher manganese average oxidation states (AOS) for the outer (S-A) surface in comparison with the inner (S-S) surface.

Based on the experimental results, it was suggested that the formation of microtubes during drying occurs due to the emergence of mechanical forces caused by the difference in surface stress values at the “upper” and “lower” surfaces of the film. These differences arise both due to the density gradient of the film substance in the transverse direction, and the difference in the chemical composition.

3.2.3. Synthesis of fluoride microtubes as a result of a reaction with hydrogen fluoride

Significant results were obtained when aqueous solutions of lanthanide salts were treated with gaseous HF [34,35,63]. As is known, the interaction of these reagents results in the formation of nanocrystals comprised of sparingly soluble fluorides, and these reagents are relatively widely used in preparative chemistry. The first experiments to obtain lanthanide fluoride microtubes by GSIT using lanthanum salt solutions with a concentration of 0.001–0.01 M and gaseous HF evaporating from the surface of a hydrofluoric acid solution showed [34] that the lanthanum fluoride film was hydrophobic, and after the reaction it was localized on the surface of the salt solution. At constant concentrations and temperature of the reagents, the thickness of such a film depends on the processing time and can reach 2–3 μm . Subsequent air-drying of this film leads to its twisting (Fig. 7a) into microtubes with a diameter from 80 to 100 μm and a length of up to 2 mm (Fig. 7b). It is shown (Fig. 7c) that the tube wall consists of an array of LaF_3 nanocrystals with a morphology of 7–15 nm thick nanosheets, with the surface area of each varying from 0.5 to 2.5 μm^2 and their packing density decreasing along the depth of the synthesized layer towards the solution. It is assumed that the formation of microtubes occurs due to

the forces of “tightening” that emerge when the lower part of the layer, which is less dense in the wet state, is being dried (Fig. 7d). Therefore, the peculiar structure of the layer and the gradient of the moisture are the driving forces of the rolling process.

3.2.4. Synthesis of microtubes as a result of reaction with ammonium

The formation of insoluble metal oxides or hydroxides layers is also observed when the solutions of corresponding salts are treated with gaseous ammonia [36]. In this case, the formation of a layer at the interface occurs as a result of the reaction of controlled hydrolysis. The driving parameters in the synthesis are not only the characteristics of the solution (pH, concentration, surfactant, etc.), but also the conditions and rate of diffusion of the gas into the solution. An example of such a synthesis is the formation of a film containing Fe_3O_4 nanoparticles in the amorphous $\text{Fe}(\text{OH})_3$ matrix. It occurs on the surface of a solution containing FeCl_2 and FeCl_3 mixture. It is reported [65] that it is possible not only to synthesize individual randomly located microtubes with a diameter from 5 to 100 μm and a length from 100 μm up to 2 mm, but also to obtain arrays of oriented magnetic microtubes (Fig. 8a). The study of its morphology by SEM showed that the tube wall has a non-uniform structure, namely, the outside surface has pores with a size of about 100 nm, and the inside surface of the wall is formed by spherical nanoparticles with a diameter of up to 10 nm (Fig. 8b and c). The TEM and HRTEM images of the tube wall are presented in Fig. 8d and e, which confirm the polycrystalline nature of the microtubes. The driving force of the “twisting” process in this case is the gradient of the particles packing density over the layer thickness. It is noted that when a certain thickness is exceeded in the resulting layer, the specified density and humidity gradient becomes insufficient for the mechanical transformation of the planar layer into tubular structures (Fig. 8f).

When ascorbic acid (a complexing agent of Fe^{2+} cations), which increases their stability with respect to the interaction with atmospheric oxygen, was added to the solution in a small quantity, an amorphous hydroxide compound layer was formed at the interface with a large difference in the AOSs of iron on both sides of the layer [37]. This difference leads to the formation of multi-wall microtubes (Fig. 8g and h).

If drying is performed not at room temperature, but at 80–130 $^\circ\text{C}$ in air, a “self-disassembly” into pieces of 8–15 μm with the formation of microscrolls (microspirals) can be observed [66]. Moreover, the possibility of obtaining metallic tubular microstructures as a result of high-

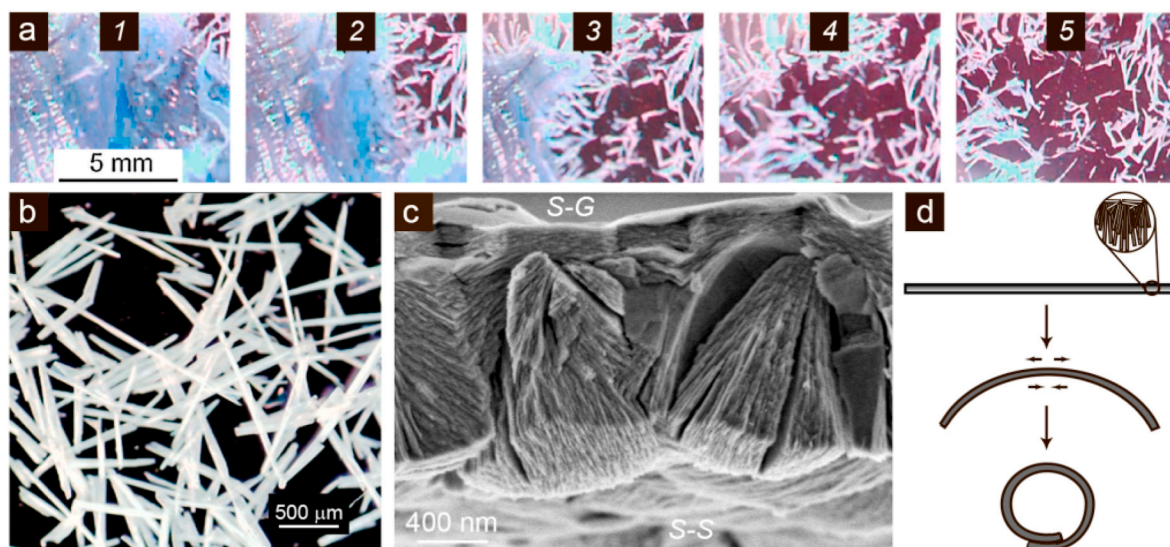


Fig. 7. Experimental results of the synthesis of LaF_3 microtubes. (a) Series of successive images during the spontaneous rolling process. Images 1–5 were taken at 0, 10, 20, 30 and 40 s, respectively. Reproduced with permission [35]. Copyright 2015, Elsevier B.V. (b) Optical microscope image of LaF_3 tubes. Reproduced with permission [64]. Copyright 2016, Elsevier B.V. (c) SEM image of the cross view of the LaF_3 microtube wall. S-G, solid-gas interface side; S-S, solid-solution interface side. Reproduced with permission [35]. Copyright 2015 Elsevier B.V. (d) Hypothetical scheme of microtube formation in the course of drying. Reproduced with permission [34]. Copyright Pleiades Publishing, Ltd.

temperature reduction in a hydrogen atmosphere, was confirmed for spirals [66] and tubes [37].

4. Possible practical uses of microtubes synthesized by GSIT

Microtubes prepared at the gas-solution interface represent truly designer science, where the tubes aspect ratio, materials compositions,

combinations and wall thicknesses can lead to novel properties, effects and functions. GSIT-synthesized tubes similar to previously shown rolled-up microtubes can be used as on- and off-chip integrated elements such as optical resonators, meta-materials, chemical sensors, catalytic motors, electronics, transport of fluids, batteries and supercapacitors. Several promising application areas for microtubes synthesized by GSIT are shown in Fig. 9.

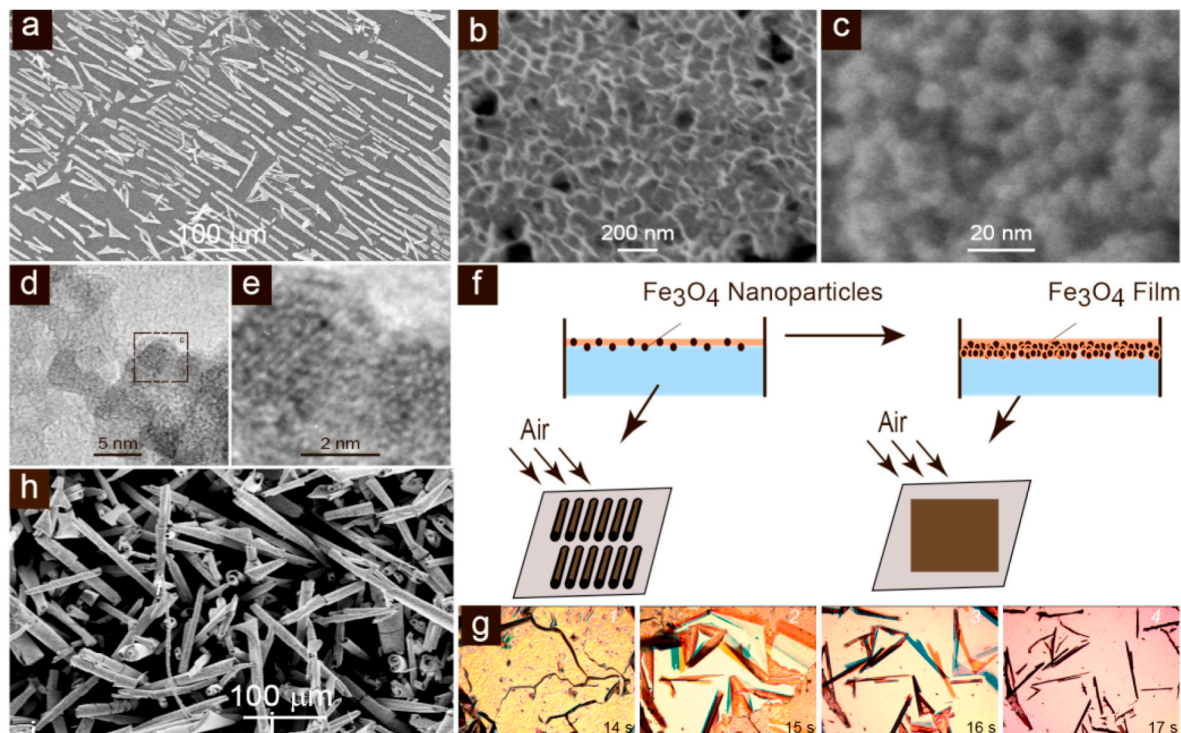


Fig. 8. Experimental results of synthesis of oxide (hydroxide) microtubes. (a–c) SEM images of Fe_3O_4 oriented microtubes: (a) general view, (b) view of the outer side of microtube, (c) view of the inner side of microtube. (d, e) TEM images of the tube wall with different magnification. (a–e) Reproduced with permission [65]. Copyright 2019, Springer Nature. (f) Hypothetical schema of the formation of Fe_3O_4 tubes and films. (g) Series of successive images during the spontaneous rolling process of the $\text{Fe}(\text{OH})_3$ layers. The images (1–4) were taken at 14, 15, 16, and 17 s. (h) SEM images of $\text{Fe}(\text{OH})_3$ microtubes. (g–h) Reproduced with permission [37]. Copyright 2018, John Wiley and Sons.

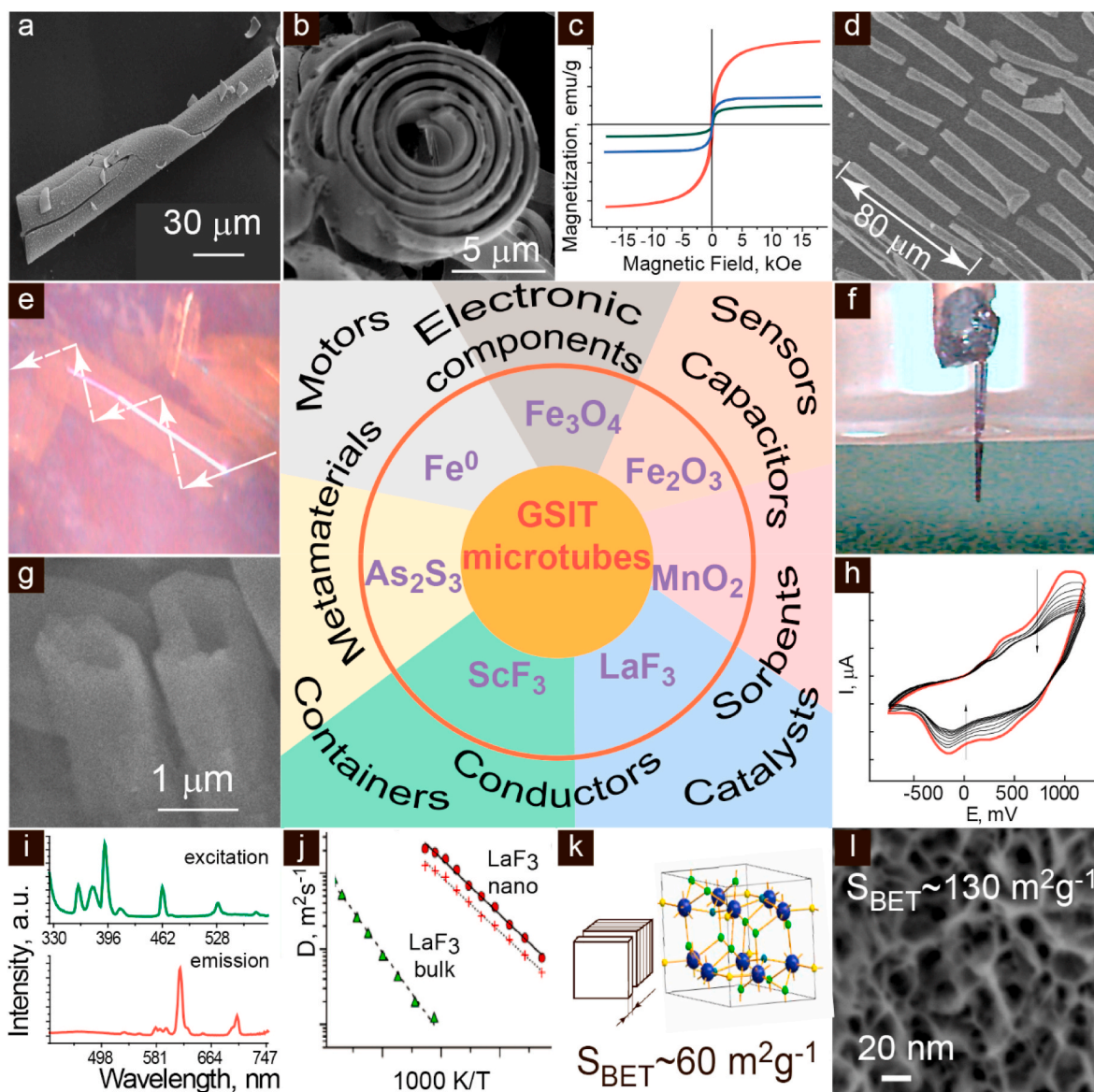


Fig. 9. Areas of possible practical use of microtubes synthesized by GSIT. The ideas for images c, d, e, h, i, j were taken from Refs. [33,36,63,65,71,78] correspondingly.

As has been mentioned before, a significant difference of GSIT microtubes from other rolled-up inorganic tubes is its crystalline structure. Tubular materials with walls consisting of 2D crystals have extremely high specific surface values. This circumstance allows obtaining nanocrystalline materials with improved functional characteristics. It is shown [63] that the fluorine self-diffusion coefficient of the nanostructured LaF_3 is about $6 \cdot 10^{-12} \text{ m}^2/\text{s}$ at 800 K (Fig. 9j), which is two orders of magnitude higher than that of the bulk LaF_3 [67]. In Refs. [68], the influence of LaF_3 nanosheets thickness on the fluorine dynamics was analyzed by NMR diffusometry, and it was established that fluorine diffusion depended on the thickness of 2D crystals (Fig. 9k). Moreover, a decrease in thickness from 18 nm to 6 nm results in an activation energy decrease from 0.76 eV to 0.23 eV. In addition, GSIT readily allows adding extra components to the material to improve its functional characteristics. It is known [69] that the doping of bulk LaF_3 with tysonite crystalline structure by SrF_2 leads to an increase in the mobility of fluorine atoms. This technique turned out to be relevant for the $\text{La}_{0.95}\text{Sr}_{0.05}\text{F}_{2.95}$ microtubular material with increased fluoride mobility [64]. Lanthanum fluoride is an important material not only for ionics, but also for optics [70]: $\text{LaF}_3:\text{Eu}^{3+}$ doped nanocrystals synthesized by GSIT can be used as luminescent material [71] (Fig. 9i).

Specific surface value (Fig. 9l) is the one of the most important property of sorbents, catalysts, capacitors, sensors [72,73]. Various inorganic oxide and hydroxide nanostructures with tubular morphology are of particular interest for electrochemical energy storage application [74–77], designing of sensors [78] (Fig. 9f,h) and treatment of wastewater [79].

Controlling the thermal expansion of materials is also of great technological importance. Famously [80,81], ScF_3 belongs to a class of materials with negative thermal expansion (NTE). It has been suggested [82] to apply the GSIT method for the synthesis of scandium fluoride microtubes with a diameter of up to 1 μm and a thickness of the tube wall from 25 to 70 nm (Fig. 9g). They can find application in the design of materials with NTE, transparent optical components, transport or safety containers; for example, to provide protection for highly sensitive units in microelectronic systems against thermal variation.

With continuous scaling of electronic technology, the miniaturization of components is an important development direction. Microtubular structures can be used as micromagnets for the precise position for robotics and microfluidic applications [83], as antenna, inductor, actuator, oscillator, and switch in NEMS or MEMS [84] (Fig. 9b–d). One of the most promising directions for the use of inorganic microtubes is the area of micromachines

or micromotors creation, actively developing in recent years, which are capable to perform mechanical movement as a result of energy conversion [85] (Fig. 9a). Just as a set of molecules in nature provides vital macro-processes, so miniature 3D arrays of hollow tubular structures integrated into functional devices and systems enable new properties, effects and functions. The study of microtubes' real applications is currently a highly relevant topic; here we have discussed several examples of materials properties that are definitely linked to tubular microstructures. The GSIT opens up new prospects for an easy synthesis of such inorganic materials with a wide range of potential applications.

5. Conclusion and further development

The examples of microtubes synthesized under GSIT conditions including oxides, fluorides and sulfides of a number of metals clearly demonstrate the distinctive features and capabilities of the method. These features include the experimental simplicity, the availability of the reagents used, the unique possibility of obtaining multicomponent compositions, and, for many of them, the unique morphology and orientation of the nanocrystals forming the walls of the microtubes. These features determine a high potential for the practical application of such microtubes. There is no doubt that they can be used as active elements of various sensors and electrochemical devices, metamaterials, active adsorbents of heavy metals, etc.

However, it should be noted that there are some problems with making such microtubes by the GSIT method, the most serious of which is the obtaining of the desirable diameter and length. After synthesis, one has to make an additional casting among an array of microtubes of different diameters. In order to obtain microtubes of the required length, it is necessary to cut and shorten them using, for example, focused ion beams. Further development of the method is likely to go towards solving some of these problems.

Nevertheless, it is important to note that for several compositions of microtubes (lanthanide fluorides, for example) the GSIT is practically the only applicable method, which makes it unique. It can be argued that it is this feature that offers great potential for its use in many advanced materials in future. Moreover, the range of compositions obtained using this method can be significantly expanded. There is no doubt that with the development of preparative chemistry, specific conditions will be discovered for acquiring a multitude of microtubes with new compositions and unique properties.

Declaration of competing interest

The authors declare that they have no known competing financial interests or personal relationships that could have appeared to influence the work reported in this paper.

Acknowledgements

This work was supported by the Russian Science Foundation (grant No. 16-13-10223-P).

Appendix A. Supplementary data

Supplementary data related to this article can be found at <https://doi.org/10.1016/j.pnsc.2020.05.001>.

References

- [1] K. Kim, J. Guo, X. Xu, D.L. Fan, *Small* 11 (2015) 4037–4057, <https://doi.org/10.1002/sml.201500407>.
- [2] R.K. Joshi, J.J. Schneider, *Chem. Soc. Rev.* 41 (2012) 5285–5312, <https://doi.org/10.1039/c2cs35089k>.
- [3] H. Zhou, Z. Ryan Tian, *Prog. Nat. Sci. Mater. Int.* 23 (2013) 273–285, <https://doi.org/10.1016/j.pnsc.2013.05.005>.
- [4] V. Luchnikov, M. Stamm, C. Akhmaliev, L. Bischoff, B. Schmidt, *J. Micromech. Microeng.* 16 (2006) 1602–1605, <https://doi.org/10.1088/0960-1317/16/8/022>.
- [5] Q. Liu, I.A. Krikunov, Z. Wang, R. Graeff, H.C. Lee, Q. Hao, *J. Phys. Chem. B* 112 (2008) 14682–14686, <https://doi.org/10.1021/jp807990g>.
- [6] R.J. Jackman, S.T. Brittain, A. Adams, H. Wu, M.G. Prentiss, S. Whitesides, G.M. Whitesides, *Langmuir* 15 (1999) 826–834, <https://doi.org/10.1021/la980857y>.
- [7] M. Vaezi, H. Seitz, S. Yang, *Int. J. Adv. Manuf. Technol.* 67 (2013) 1721–1754, <https://doi.org/10.1007/s00170-012-4605-2>.
- [8] H. Lu, K. Yan, J. Yan, J. Wang, B. Huang, *Mater. Chem. Phys.* 110 (2008) 136–139, <https://doi.org/10.1016/j.matchemphys.2008.01.026>.
- [9] S.S.N. Bharadwaja, M. Olszta, S. Trolier-McKinstry, X. Li, T.S. Mayer, F. Roozeboom, *J. Am. Ceram. Soc.* 89 (2006) 2695–2701, <https://doi.org/10.1111/j.1551-2916.2006.01123.x>.
- [10] R. Wang, D. Chen, L. Ren, J. Guo, T. Liu, *J. Mater. Res.* 26 (2011) 1072–1075, <https://doi.org/10.1557/jmr.2011.75>.
- [11] D. Yan, Y. Feng, C. Wang, *Prog. Nat. Sci. Mater. Int.* 23 (2013) 543–548, <https://doi.org/10.1016/j.pnsc.2013.11.008>.
- [12] A.A. Krasilin, A.M. Suprun, E.V. Ubyvovik, V.V. Gusarov, *Mater. Lett.* 171 (2016) 68–71, <https://doi.org/10.1016/j.matlet.2016.01.152>.
- [13] A.A. Krasilin, V.N. Nevedomsky, V.V. Gusarov, *J. Phys. Chem. C* 121 (2017) 12495–12502, <https://doi.org/10.1021/acs.jpcc.7b03785>.
- [14] V. Reedo, M. Järvekülg, A. Lõhmus, U. Mäeorg, *Phys. Status Solidi* 205 (2008) 1511–1514, <https://doi.org/10.1002/pssa.200778165>.
- [15] Y. Lu, C. Liu, W. Peng, *J. Eng.* 2016 (2016) 266–268, <https://doi.org/10.1049/joe.2016.0162>.
- [16] A.E. Paz y Puente, D.C. Dunand, *Intermet* 92 (2018) 42–48, <https://doi.org/10.1016/j.intermet.2017.09.010>.
- [17] G. Huang, Y. Mei, *Adv. Mater.* 24 (2012) 2517–2546, <https://doi.org/10.1002/adma.201200574>.
- [18] V.Y. Prinz, V.A. Seleznev, A.K. Gutakovskiy, A.V. Chehovskiy, V.V. Preobrazhenskii, M.A. Putyato, T.A. Gavrilova, *Phys. E* 6 (2000) 828–831, [https://doi.org/10.1016/S1386-9477\(99\)00249-0](https://doi.org/10.1016/S1386-9477(99)00249-0).
- [19] C.H. Xu, X. Wu, G.S. Huang, Y.F. Mei, *Adv. Mater. Technol.* 4 (2019) 1800486, <https://doi.org/10.1002/admt.201800486>.
- [20] Q. Guo, Z. Di, M.G. Lagally, Y. Mei, *Mater. Sci. Eng. R* 128 (2018) 1–31, <https://doi.org/10.1016/j.mser.2018.02.002>.
- [21] F. Cavallo, R. Songmuang, C. Ulrich, O.G. Schmidt, *Appl. Phys. Lett.* 90 (2007) 193120, <https://doi.org/10.1063/1.2737425>.
- [22] Y. Mei, G. Huang, A.A. Solovev, E.B. Ureña, I. Mönch, F. Ding, T. Reindl, R.K.Y. Fu, P.K. Chu, O.G. Schmidt, *Adv. Mater.* 20 (2008) 4085–4090, <https://doi.org/10.1002/adma.200801589>.
- [23] E.W.H. Jager, E. Smela, O. Inganas, *Science* 290 (2000) 1540–1545, <https://doi.org/10.1126/science.290.5496.1540>.
- [24] B.R. Xu, Z. Tian, J. Wang, H. Han, T. Lee, Y.F. Mei, *Sci. Adv.* 4 (2018) eaap8203, <https://doi.org/10.1126/sciadv.aap8203>.
- [25] C. Zhou, R. Shi, L. Shang, L.-Z. Wu, C.-H. Tung, T. Zhang, *Nano Res* 11 (2018) 3462–3468, <https://doi.org/10.1007/s12274-018-2003-2>.
- [26] R. Streubel, J. Lee, D. Makarov, M.Y. Im, D. Karnauschenko, L. Han, R. Schäfer, P. Fischer, S.K. Kim, O.G. Schmidt, *Adv. Mater.* 26 (2014) 316–323, <https://doi.org/10.1002/adma.201303003>.
- [27] R. Sharma, C.C.B. Bufon, D. Grimm, R. Sommer, A. Wollatz, J. Schadowald, D.J. Thurmer, P.F. Siles, M. Bauer, O.G. Schmidt, *Adv. Energy Mater.* 4 (2014) 1301631, <https://doi.org/10.1002/aenm.201301631>.
- [28] D. Grimm, C.C. Bof Bufon, C. Deneke, P. Atkinson, D.J. Thurmer, F. Schäffel, S. Gorantla, A. Bachmatiuk, O.G. Schmidt, *Nano Lett.* 13 (2013) 213–218, <https://doi.org/10.1021/nl303887b>.
- [29] W. Huang, X. Yu, P. Froeter, R. Xu, P. Ferreira, X. Li, *Nano Lett.* 12 (2012) 6283–6288, <https://doi.org/10.1021/nl303395d>.
- [30] A.A. Solovev, Y. Mei, E.B. Ureña, G. Huang, O.G. Schmidt, *Small* 5 (2009) 1688–1692, <https://doi.org/10.1002/sml.200900021>.
- [31] J. Wang, T. Zhan, G. Huang, P.K. Chu, Y. Mei, *Laser Photon. Rev.* 8 (2014) 521–547, <https://doi.org/10.1002/lpor.201300040>.
- [32] Y. Fang, X. Lin, S. Tang, B. Xu, J. Wang, Y. Mei, *Prog. Nat. Sci. Mater. Int.* 27 (2017) 498–502, <https://doi.org/10.1016/j.pnsc.2017.03.011>.
- [33] V.P. Tolstoy, L.B. Gulina, *J. Nano-Electron. Phys.* 5 (2013) 01003.
- [34] L.B. Gulina, V.P. Tolstoy, *Russ. J. Gen. Chem.* 84 (2014) 1472–1475, <https://doi.org/10.1134/S1070363214080039>.
- [35] L.B. Gulina, V.P. Tolstoy, I.A. Kasatkin, Y.V. Petrov, *J. Fluor. Chem.* 180 (2015) 117–121, <https://doi.org/10.1016/j.jfluchem.2015.09.002>.
- [36] V.E. Gurenko, V.P. Tolstoy, L.B. Gulina, *Nanosyst.-Phys. Chem. Math.* 8 (2017) 471–475, <https://doi.org/10.17586/2220-8054-2017-8-4-471-475>.
- [37] L. Gulina, V. Tolstoy, L. Kuklo, V. Mikhailovskii, V. Panchuk, V. Semenov, *Eur. J. Inorg. Chem.* 2018 (2018) 1842–1846, <https://doi.org/10.1002/ejic.201800182>.
- [38] V.P. Tolstoy, L.B. Gulina, *Langmuir* 30 (2014) 8366–8372, <https://doi.org/10.1021/la501204k>.
- [39] H. Kierzkowska-Pawlak, *Ecol. Chem. Eng. S.* 19 (2012) 175–196, <https://doi.org/10.2478/v10216-011-0014-y>.
- [40] P.D. Vaidya, E.Y. Kenig, *Chem. Eng. Commun.* 194 (2007) 1543–1565, <https://doi.org/10.1080/00986440701518314>.
- [41] K.J. Edler, *Soft Matter* 2 (2006) 284–292, <https://doi.org/10.1039/b514420e>.
- [42] Y. Chen, C. Yang, X. Wang, J. Yang, K. Ouyang, J. Li, *J. Mater. Chem. A* 4 (2016) 10345–10351, <https://doi.org/10.1039/c6ta03314h>.
- [43] D. Kisailus, B. Schwenzler, J. Gomm, J.C. Weaver, D.E. Morse, *J. Am. Chem. Soc.* 128 (2006) 10276–10280, <https://doi.org/10.1021/ja062434l>.
- [44] Z. Shi, A. Zhang, Q. Zhang, *Cryst. Res. Technol.* 49 (2014) 837–844, <https://doi.org/10.1002/crat.201400124>.

- [45] Y. He, Q. Sheng, B. Liu, J. Zheng, *Electrochim. Acta* 66 (2012) 82–87, <https://doi.org/10.1016/j.electacta.2012.01.045>.
- [46] Q.H. Yuan, Z.W. Lu, P.X. Zhang, X.B. Luo, X.Z. Ren, *Chin. J. Inorg. Chem.* 28 (2012) 1429–1434.
- [47] J. Zhao, Z. Shi, Q. Zhang, *J. Alloys Compd.* 668 (2016) 176–186, <https://doi.org/10.1016/j.jallcom.2016.01.186>.
- [48] W. Bai, Q. Sheng, F. Nie, J. Zheng, *ACS Appl. Mater. Interfaces* 7 (2015) 28377–28386, <https://doi.org/10.1021/acsami.5b09094>.
- [49] J. Liu, W. Bai, J. Zhang, J. Zheng, *Anal. Methods* 8 (2016) 7903–7909, <https://doi.org/10.1039/c6ay02376b>.
- [50] Z. Yang, C. Qi, X. Zheng, J. Zheng, *Talanta* 140 (2015) 198–203, <https://doi.org/10.1016/j.talanta.2015.03.023>.
- [51] L.B. Gulina, V.P. Tolstoy, E.V. Tolstobrov, *Mendeleev Commun.* 27 (2017) 634–636, <https://doi.org/10.1016/j.mencom.2017.11.033>.
- [52] L.B. Gulina, V.P. Tolstoy, I.A. Kasatkin, S.A. Fateev, *J. Mater. Sci.* 53 (2018) 8161–8169, <https://doi.org/10.1007/s10853-018-2164-0>.
- [53] S.H. Pawar, S. Tamhankar, P.N. Bhosale, M.D. Uplane, *Indian J. Pure Appl. Phys.* 21 (1983) 665–667.
- [54] S.H. Pawar, P.N. Bhosale, M.D. Uplane, S. Tamhankar, *Thin Solid Films* 110 (1983) 165–170, [https://doi.org/10.1016/0040-6090\(83\)90220-1](https://doi.org/10.1016/0040-6090(83)90220-1).
- [55] X. Lu, F. Pu, Y. Xia, W. Huang, Z. Li, *Appl. Surf. Sci.* 299 (2014) 131–135, <https://doi.org/10.1016/j.apsusc.2014.01.196>.
- [56] G.-Q. Xin, H.-P. Ding, Y.-G. Yang, S.-L. Shen, Z.-C. Xiong, X. Chen, J. Hao, H.-G. Liu, *Cryst. Growth Des.* 9 (2009) 2008–2012, <https://doi.org/10.1021/cg800717j>.
- [57] H. Yang, N. Coombs, G.A. Ozin, *J. Mater. Chem.* 8 (1998) 1205–1211, <https://doi.org/10.1039/a800004b>.
- [58] X.-H. Guo, S.-H. Yu, Y. Lu, G.-B. Yuan, M. Sedláč, H. Cölfen, *Langmuir* 26 (2010) 10102–10110, <https://doi.org/10.1021/la1002308>.
- [59] A.S. Schenk, S. Eiben, M. Goll, L. Reith, A.N. Kulak, F.C. Meldrum, H. Jeske, C. Wege, S. Ludwigs, *Nanoscale* 9 (2017) 6334–6345, <https://doi.org/10.1039/c7nr00508c>.
- [60] L. Gulina, V. Tolstoy, *Micro- and nanotubes of As₂S₃ and AgAs₂ synthesized in "soft" chemistry conditions*, in: O.F. Vyvenko (Ed.), *State-of-the-art Trends of Scientific Researches of Artificial and Natural Nanoobjects, STRANN-2011*, Saint-Petersburg State University, Saint-Petersburg, Russia, 2011, p. 91.
- [61] M.S. Iovu, S.D. Shutov, A.M. Andriesh, E.I. Kamitsos, C.P.E. Varsamis, D. Furniss, A.B. Seddon, M. Popescu, *J. Optoelectron. Adv. Mater.* 3 (2001) 443–454.
- [62] V.P. Tolstoy, L.B. Gulina, *Russ. J. Gen. Chem.* 83 (2013) 1635–1639, <https://doi.org/10.1134/S1070363213090016>.
- [63] L.B. Gulina, M. Schäfer, A.F. Privalov, V.P. Tolstoy, I.V. Murin, *J. Chem. Phys.* 143 (2015) 234702, <https://doi.org/10.1063/1.4937415>.
- [64] L.B. Gulina, M. Schäfer, A.F. Privalov, V.P. Tolstoy, I.V. Murin, M. Vogel, *J. Fluor. Chem.* 188 (2016) 185–190, <https://doi.org/10.1016/j.jfluchem.2016.07.006>.
- [65] V. Gurenko, L. Gulina, V. Tolstoy, *J. Sol. Gel Sci. Technol.* (2019), <https://doi.org/10.1007/s10971-019-04949-w>.
- [66] L.B. Gulina, V.P. Tolstoy, A.A. Lobinsky, Y.V. Petrov, *Syst. Charact.* 35 (2018) 1800186, <https://doi.org/10.1002/ppsc.201800186>.
- [67] A.F. Privalov, I.V. Murin, *Phys. Solid State* 41 (1999) 1482–1485, <https://doi.org/10.1134/1.1131036>.
- [68] L.B. Gulina, M. Schikora, A.F. Privalov, M. Weigler, V.P. Tolstoy, I.V. Murin, M. Vogel, *Appl. Magn. Reson.* 50 (2019) 579–588, <https://doi.org/10.1007/s00723-018-1077-z>.
- [69] N.I. Sorokin, M.V. Fominykh, E.A. Krivandina, Z.I. Zhmurova, B.P. Sobolev, O.I. Lyamina, *Phys. Solid State* 40 (1998) 604–607, <https://doi.org/10.1134/1.1130362>.
- [70] P.P. Fedorov, A.A. Luginina, S.V. Kuznetsov, V.V. Osiko, *Nanofluorides*, *J. Fluorine Chem.* 132 (2011) 1012–1039, <https://doi.org/10.1016/j.jfluchem.2011.06.025>.
- [71] L.B. Gulina, V.P. Tolstoy, I.A. Kasatkin, I.E. Kolesnikov, D.V. Danilov, *J. Fluor. Chem.* 200 (2017) 18–23, <https://doi.org/10.1016/j.jfluchem.2017.05.006>.
- [72] E. Masika, R. Mokaya, *Prog. Nat. Sci. Mater. Int.* 23 (2013) 308–316, <https://doi.org/10.1016/j.pnsc.2013.04.007>.
- [73] W. Yue, W. Zhou, *Prog. Nat. Sci. Mater. Int.* 18 (2008) 1329–1338, <https://doi.org/10.1016/j.pnsc.2008.05.010>.
- [74] A. Numan, N. Duraisamy, F. Saiha Omar, D. Gopi, K. Ramesh, S. Ramesh, *Prog. Nat. Sci. Mater. Int.* 27 (2017) 416–423, <https://doi.org/10.1016/j.pnsc.2017.06.003>.
- [75] H. Xiao, S. Yao, H. Liu, F. Qu, X. Zhang, X. Wu, *Prog. Nat. Sci. Mater. Int.* 26 (2016) 271–275, <https://doi.org/10.1016/j.pnsc.2016.05.007>.
- [76] Y. Xu, Z. Liu, D. Chen, Y. Song, R. Wang, *Prog. Nat. Sci. Mater. Int.* 27 (2017) 197–202, <https://doi.org/10.1016/j.pnsc.2017.03.001>.
- [77] G. Zhu, J. Yang, Y. Liu, X. Xie, Z. Ji, J. Yin, X. Shen, *Prog. Nat. Sci. Mater. Int.* 26 (2016) 264–270, <https://doi.org/10.1016/j.pnsc.2016.05.016>.
- [78] V.P. Tolstoy, L.B. Gulina, A.A. Golubeva, S.S. Ermakov, V.E. Gurenko, D.V. Navolotskaya, N.I. Vladimirova, A.V. Koroleva, *J. Solid State Electrochem.* 23 (2019) 573–582, <https://doi.org/10.1007/s10008-018-04165-6>.
- [79] R. Zhao, J. Xu, P. Tao, F. Shi, F. Yu, X. Zeng, C. Song, J. Wu, W. Shang, T. Deng, *Prog. Nat. Sci. Mater. Int.* 28 (2018) 422–429, <https://doi.org/10.1016/j.pnsc.2018.05.005>.
- [80] L. Hu, J. Chen, A. Sanson, H. Wu, C. Guglieri Rodriguez, L. Olivi, Y. Ren, L. Fan, J. Deng, X. Xing, *J. Am. Chem. Soc.* 138 (2016) 8320–8323, <https://doi.org/10.1021/jacs.6b02370>.
- [81] I.A. Kasatkin, L.B. Gulina, N.V. Platonova, V.P. Tolstoy, I.V. Murin, *CrystEngComm* 20 (2018) 2768–2771, <https://doi.org/10.1039/C8CE00257F>.
- [82] L.B. Gulina, V.P. Tolstoy, Y.V. Petrov, D.V. Danilov, *Inorg. Chem.* 57 (2018) 9779–9781, <https://doi.org/10.1021/acs.inorgchem.8b01375>.
- [83] A. Khosla, J.L. Korčok, B.L. Gray, D.B. Leznoff, J.W. Herchenroeder, D. Miller, Z. Chen, *Proc. SPIE* 7593 (2010) 759316, <https://doi.org/10.1117/12.840942>.
- [84] C.H. Ahn, M.G. Allen, *J. Micromech. Microeng.* 3 (1993) 37–44, <https://doi.org/10.1088/0960-1317/3/2/001>.
- [85] T. Xu, W. Gao, L.P. Xu, X. Zhang, S. Wang, *Adv. Mater.* 29 (2017) 1603250, <https://doi.org/10.1002/adma.201603250>.